

## EXPOSING THE GAS BRAKING MECHANISM OF THE $\beta$ PICTORIS DISK\*

ALEXIS BRANDEKER

Dept. of Astronomy, Stockholm University, SE-106 91 Stockholm, Sweden

Draft version June 9, 2018

### ABSTRACT

Ever since the discovery of the edge-on circumstellar disk around  $\beta$  Pictoris, a standing question has been why the gas observed against the star in absorption is not rapidly expelled by the strong radiation pressure from the star. A solution to the puzzle has been suggested to be that the neutral elements that experience the radiation force also are rapidly ionized, and so are only able to accelerate to an average limiting velocity  $v_{\text{ion}}$ . Once ionized, the elements are rapidly braked by C II, which is observed to be at least  $20\times$  overabundant in the disk with respect to other species. A prediction from this scenario is that different neutral elements should reach different  $v_{\text{ion}}$ , depending on the ionization thresholds and strengths of driving line transitions. In particular, neutral Fe and Na are predicted to reach the radial velocities  $0.5$  and  $3.3\text{ km s}^{-1}$ , respectively, before being ionized. In this paper we study the absorption profiles of Fe and Na from the circumstellar gas disk around  $\beta$  Pic, as obtained by HARPS at the ESO 3.6 m telescope. We find that the Fe and Na velocity profiles are indeed shifted with respect to each other, confirming the model. The absence of an extended blue wing in the profile of Na, however, indicates that there must be some additional braking on the neutrals. We explore the possibility that the ion gas (dominated by C II) can brake the neutrals, and conclude that about  $2\text{--}5\times$  more C than previously estimated is needed for the predicted line profile to be consistent with the observed one.

*Subject headings:* circumstellar matter – protoplanetary disks – stars: formation – stars: individual ( $\beta$  Pictoris)

### 1. INTRODUCTION

Understanding the evolution of gas in circumstellar (CS) disks is critical to understand star and planet formation. Unfortunately, CS gas in general is very difficult to observe, so how and when the gas disappears, is still poorly known. The main difficulty is that the cool gas in disks only thermally excites the lowest lying energy levels, which emit radiation in mid- to far-infrared wavelengths that are blocked by the terrestrial atmosphere. Radiatively excited levels are easily observed from the ground, but require very high contrast sensitivity, as the star typically emits many orders of magnitude more radiation at the same wavelengths. In the case the CS disk is seen edge on, however, the gas can be seen in absorption against the star. This is the case for the disk around  $\beta$  Pictoris, where CS absorption lines were found (Slettebak 1975) long before the disk was discovered (Aumann 1985; Smith & Terrile 1984).  $\beta$  Pic is a nearby ( $19.44\pm 0.05\text{ pc}$ ; van Leeuwen 2007) A5 main-sequence star estimated to be  $10\text{--}20\text{ Myr}$  old (Zuckerman et al. 2001; Mentuch et al. 2008). Because time scales for dust removal mechanisms are much shorter than the age of the system (Backman & Paresce 1993), the dust disk must be replenished. The most popular mechanism to replenish the dust disk is through collisional cascades from planetesimal size objects, hence the classification of the  $\beta$  Pic disk as a *debris* disk.

Even though the fate of CS gas is much less constrained than the dust, also the gas disk around  $\beta$  Pic is thought to be secondary as opposed to a remnant from the star forming nebula, as indicated by the pres-

ence of CO (Vidal-Madjar et al. 1994) that quickly is dissociated (van Dishoeck & Black 1988), and by dynamical arguments (Fernández, Brandeker, & Wu 2006, hereafter FBW06). Suggested mechanisms for replenishing the gas are photo-desorption of dust (Chen et al. 2007), evaporation of comets (Beust et al. 1989), and collisional evaporation of dust grains (Czechowski & Mann 2007).

After the discovery of the  $\beta$  Pic CS dust disk, more attention was directed towards the gas observed in absorption against the star (Hobbs et al. 1985), and it was soon realized that the expelling radiation force on many elements exceed the gravity — by up to a factor of several hundred in the case of Na I. Yet, most of the gas absorption is observed to be at rest with respect to the star. Evidently, there must be some braking agent at work, but the lack of spatial information of the location of the gas made it difficult to constrain braking models — e.g. Lagrange et al. (1998) suggested that a dense ring of H I at sub-AU distance from the star would be able to brake the gas through friction, without violating any observational constraints known at the time. This changed with the detection of spatially resolved Na I emission from the disk, observed to be co-located with the dust disk out to hundreds of AU (Olofsson et al. 2001). For H to brake the Na I over the whole disk, Brandeker et al. (2004) estimated that the required mass would have to be higher than upper limits set on H I (Freudling et al. 1995) and H<sub>2</sub> (Lecavelier des Etangs et al. 2001).

The problem of how the gas around  $\beta$  Pic is braked was investigated in detail by FBW06. One key observation they made was that all neutrals that are subject to a strong radiation force, are also quickly ionized. The neutrals thus only reach small velocities  $v_{\text{ion}}$  on average (depending on element) before being ionized. Since ions

\* Based on observations made with ESO Telescopes at the La Silla Observatory.

are affected by long-range Coulomb forces, they interact strongly and act as a single fluid; ions experiencing radiation force are efficiently braked by those unaffected by radiation. For ions, C II turns out to be the most dominant braking agent, while Fe II is the strongest driver. For gas of cosmic abundance, the effective radiation force acting on the gas as a whole, was found to be  $4\times$  stronger than gravity. In effect, Fe II would drag the rest of the gas along and expel it from the system. In order for the ion gas to be stable against the radiation pressure, an overabundance of at least  $10\times$  of C would be required, and in fact, FUSE observations of C in absorption against the star subsequently proved C to be at least  $20\times$  overabundant, providing the stabilizing inertia to brake the disk (Roberge et al. 2006, hereafter ROB06).

A prediction from the scenario that only ions are braked, is that neutrals should be observed to reach a radial velocity of  $v_{\text{ion}}$  with respect to the star. The purpose of this paper is to test that prediction in detail, by making use of archival high spectral resolution data that has been obtained of  $\beta$  Pic for other purposes. Since the absolute heliocentric velocity of  $\beta$  Pic is very hard to measure to good accuracy we treat it as a free parameter and focus on the observed differential velocity between Fe I and Na I. The paper is organized as follows. In §2 we study what the implications of the braking scenario look like in detail, in particular the expected absorption line profiles. §3 reports on how the data we use to compare with theory were acquired and handled, especially the somewhat elaborate procedure to remove telluric lines from the Na I region. In §5 we show the resulting comparisons, and discuss implications. The paper is concluded by §6.

## 2. LINE PROFILES

If disk braking operates on ions, but not on neutrals, we can expect the neutrals to be accelerated for a short while before getting ionized. Since the number of accelerating photons outnumber the ionizing photons by at least two orders of magnitude, we can treat acceleration as a continuous process while the time before ionization is stochastic according to an exponential distribution. Given an ensemble of particles, this will give rise to a distribution of velocities at any given moment, which will broaden an absorption line and result in a characteristic profile. In the following two subsections we first study the case that there is no braking acting on the neutral particle, and then continue with the case where some braking is provided by a surrounding ion gas.

### 2.1. Freely accelerated neutrals

To find out what kind of absorption profile we should expect from neutral elements being radially accelerated, we make the following assumptions:

1. The neutral particles are ionized at a rate  $\Gamma(r) \propto r^{-2}$ , where  $r$  is the distance to the star. The particle has no “memory”; the lifetime  $\Lambda$  of a neutral particle is thus exponentially distributed with the expected lifetime  $\Gamma^{-1}$ .
2. The particles are in ionization equilibrium, meaning that the recombination rate equals the ionization rate.

3. The particles travel a very short distance before being ionized;  $r$  is thus essentially constant during the neutral phase.
4. Ionized particles are braked efficiently and so are at zero radial velocity. Neutral particles thus start with no radial velocity.

The probability density distribution of the lifetime  $\Lambda$  before ionization is thus

$$f_{\Lambda}(t) = \Gamma \exp(-\Gamma t). \quad (1)$$

The radial equation of motion for a particle when it becomes neutral is

$$m \frac{dv}{dt} = (\beta - 1) \frac{GM_{\star}m}{r^2} + \frac{mL^2}{r^3}, \quad (2)$$

where  $\beta = F_{\text{rad}}/F_{\text{grav}}$  is the ratio between radiation force  $F_{\text{rad}}$  and gravity  $F_{\text{grav}}$ ,  $G$  is the gravitational constant, and  $M_{\star}$  is the mass of the central star. The angular momentum  $L = (GM_{\star}r_0)^{1/2}$ , assuming the particle becomes neutral while in a circular Keplerian orbit of radius  $r_0$ . For a particle moving a short radial distance before becoming ionized again (and thus  $r \approx r_0$ ), the radial acceleration during its neutral lifetime can be approximated with

$$a = \beta \frac{GM_{\star}}{r^2}, \quad (3)$$

The velocity reached by a particle before ionization is then  $V_{\text{ion}} = a\Lambda$ , and its velocity probability density distribution

$$f_{V_{\text{ion}}}(v) = v_{\text{ion}}^{-1} \exp\left(-\frac{v}{v_{\text{ion}}}\right), \quad (4)$$

where we have substituted  $v \equiv at$  and  $v_{\text{ion}} \equiv a/\Gamma$  is the expected radial velocity of a particle before ionization (and so the radial dependence  $r^{-2}$  is divided out here).

Since the lifetimes are exponentially distributed, they do not depend on *when* the estimate is made, the distribution of remaining lifetime is always the same. In particular, since we have ionization equilibrium, the lifetime probability distribution is equal to the distribution of times *since recombination*. The normalized column density profile of particle density as a function of velocity  $N(v)$  is therefore equal to Eq. 4:

$$N(v) = v_{\text{ion}}^{-1} \exp\left(-\frac{v}{v_{\text{ion}}}\right). \quad (5)$$

### 2.2. Neutrals braked by ion gas

If the neutrals moving radially outwards are interacting with a gas at rest, the neutrals will be braked. The neutral-neutral interaction cross-section is tiny, however, and requires a very high gas density to be effective. Much more efficient is neutral-ion interaction, due to the polarizability of neutral elements. Since the gas around  $\beta$  Pic is strongly ionized, we now look closer on how the absorption profile would be affected from the braking.

The braking of neutrals in an ion gas is analogous to ions being braked in a neutral gas, a problem studied by Beust et al. (1989). The equation of motion for a neutral particle of mass  $m$  accelerated by radiation and braked by an ion gas is

$$m \frac{dv}{dt} = \beta \frac{GM_{\star}m}{r^2} - kv, \quad (6)$$

where

$$k = \pi \sqrt{\frac{4\alpha e^2}{4\pi\epsilon_0}} \sum_i n_i \frac{m_i}{\sqrt{\mu_i}}, \quad (7)$$

$n_i$  is the number density of ions of species  $i$ ,  $m_i$  is the ion mass,  $\mu_i = m_i m / (m_i + m)$  is the reduced mass,  $\alpha$  is the polarizability of the neutral particle,  $e$  is the electron charge, and  $\epsilon_0$  is the electrical permittivity. The asymptotic stable solution is

$$v = v_{\text{drift}} \equiv \frac{\beta G M_* m}{k r^2}. \quad (8)$$

If  $v_{\text{drift}} t_{\text{drag}} \ll r$ , where  $t_{\text{drag}} \equiv m/k$ , then the time-dependent solution is

$$v(t) \approx v_{\text{drift}} [1 - \exp(-t/t_{\text{drag}})], \quad (9)$$

where we have assumed that the particle starts without initial velocity. The probability distribution for the lifetime  $\Lambda$  of a neutral particle is still given by Eq. 1, so the resulting velocity distribution  $v(\Lambda)$  is described by the probability density distribution

$$N(v) = f_{\Lambda}(t(v)) \left| \frac{dt(v)}{dv} \right| = v_{\text{ion}}^{-1} \left( 1 - \frac{v}{\gamma v_{\text{ion}}} \right)^{(\gamma-1)}, \quad (10)$$

where  $\gamma \equiv v_{\text{drift}}/v_{\text{ion}} = \Gamma t_{\text{drag}}$ . For  $\gamma \gg 1$ , Eq. 10 reduces to Eq. 5. The expected velocity is

$$E[v] = \frac{\gamma v_{\text{ion}}}{\gamma + 1}, \quad (11)$$

which turns to

$$E[v] \approx v_{\text{ion}} \quad (12)$$

for  $\gamma \gg 1$ . From Eq. 10 follows that there generally is a radial dependence of the velocity profile (as it depends on local circumstances, such as ion gas density), in contrast to the freely accelerating profile of Eq. 5.

### 2.3. Self-shielding: numerical model

The photons that contribute to the acceleration of the gas are generally scattered in a direction different from the line of sight. This extinction implies that gas located further out will see fewer photons, resulting in a lower effective radiation force coefficient  $\beta$ ; this is called *self-shielding*. The coefficient  $\beta$  for a particle will thus depend on the column density of particles between its position and the star, of particles that share the same velocity. The  $\beta$  coefficient then in turn determines the acceleration, and what velocity the particle will reach before getting ionized. Because  $\beta$  is changing with velocity, and depends on the radial density profile of particles, we model this effect of self-shielding numerically. The numerical model is simplified by the one-dimensional nature of the problem, and that gas at outer radii are affected by gas inside, but not the reverse. For modeling the absorption profile from  $\beta$  Pic, we assume the density, ionization, and temperature distribution computed by Zagorovsky, Brandeker, & Wu (2010, hereafter ZBW10). The procedure adopted as follows:

1. Divide the radial distance into  $N_{\text{shell}}$  shells of thickness  $\Delta r$ . Start with the innermost shell and compute the velocity distribution of particles in each shell going outwards.

2. Use  $N_{\text{part}}$  number of particles in a shell (where each particle represents a number of real particles). Initialize all particles with a random thermal velocity  $v$  according to the probability distribution  $V_{\text{T}}(v) = (2\pi\sigma_{\text{T}}^2)^{-1/2} \exp[-0.5(v/\sigma_{\text{T}})^2]$ , where  $\sigma_{\text{T}} = [k_{\text{B}} T_i / m]^{1/2}$ ,  $T_i$  is the temperature of the shell  $i$ , and  $m$  is the mass of the particle. The radius of shell  $i$  is  $r_i$ .
3. Use the velocity dependent optical depth  $\tau(v)$  towards the star to compute  $\beta$  as a function of  $v$ . There is no extinction inside the first shell.
4. Iterate  $N_{\text{iter}}$  times. For each iteration, evolve the velocity of each particle according to the equation of motion of Eq. 6 using a time step of  $\Delta t \propto \Gamma_{\text{ion}}^{-1}(r_i)$ , with the addition that  $\beta$  is a function of  $v$ . For each iteration and particle, reset the particle velocity to the thermal velocity with probability  $\Gamma_{\text{ion}} \Delta t$ . This simulates that the particle gets ionized. Since we assume ionization equilibrium, there is a recombination for each ionization, and the recombined particle is set to the thermal velocity of the gas (the assumption is that ions are efficiently braked to on average  $\sim$ zero radial velocity). After  $N_{\text{iter}}$  iterations the solution has converged to a stable statistical distributions of radial velocities of the particles.
5. Make a histogram of the velocities of all particles inside the present shell, with  $N_{\text{vel}}$  velocity bins and bin size  $\Delta v$ . Normalize the distribution such that it corresponds to the total column density of the shell,  $\sum_{v_j} \Delta N_i(v_j) = n_{\text{gas}}(r_i) \Delta r$ .
6. Compute the extinction towards the star for the next shell by adding the velocity dependent column density for each shell,  $N_i(v_j) = \sum_{k \leq i} \Delta N_k(v_j)$ , and find  $\tau_i(v_j) = N_i(v_j) \sigma_0 c / (\lambda_0 \Delta v)$ , where  $\lambda_0$  is the wavelength of the transition and

$$\sigma_0 = \frac{A_{ij} \lambda_0^4 g_j}{8\pi c g_i} \quad (13)$$

is the cross-section times wavelength per particle for the transition, where  $A_{ij}$  is the Einstein coefficient and  $g_j$  and  $g_i$  the statistical weights of the levels.

7. Repeat from (2) for all shells. The observed profile can then be estimated from  $\tau_{N_{\text{shell}}}(v)$ .

We implemented this model in MATLAB for Na I around  $\beta$  Pic, and verified it by testing against conditions where the analytical profiles of §§2.1 and 2.2 should be valid, with excellent agreement. In detail, we used  $N_{\text{shell}} = 186$  with  $r_i$  between 15 and 200 AU (and thus  $\Delta r = 1$  AU),  $N_{\text{part}} = 10^4$  per shell,  $N_{\text{iter}} = 10^4$  iterations, and a time step of  $\Delta t = [2000\Gamma_{\text{ion}}(r)]^{-1}$  (meaning we iterate 5 times longer than the ionization time scale). For the velocity grid, we used  $\Delta v = 100 \text{ m s}^{-1}$  from  $-2$  to  $20 \text{ km s}^{-1}$ , to be certain to cover most of the particle velocities. For the Na I D<sub>2</sub> line  $\sigma_0 = 1.987 \times 10^{-13} \text{ cm}^2 \text{ atom}^{-1}$ , and for the D<sub>1</sub> line the cross section is 1/2 as much.

TABLE 1  
LINES STUDIED

| Element | Design.        | $\lambda_{\text{air}}[\text{\AA}]$ | $A_{ul}[\text{s}^{-1}]$ | $g_u - g_l$ | Ref. <sup>c</sup> |
|---------|----------------|------------------------------------|-------------------------|-------------|-------------------|
| Ca II   | K              | 3933.6614                          | $1.47 \times 10^8$      | 4 - 2       | 1                 |
| Ca II   | H              | 3968.4673                          | $1.4 \times 10^8$       | 2 - 2       | 1                 |
| Fe I    |                | 3824.4436                          | $2.83 \times 10^6$      | 7 - 9       | 1                 |
| Fe I    |                | 3859.9114                          | $9.70 \times 10^6$      | 9 - 9       | 1                 |
| Na I    | D <sub>2</sub> | 5889.950954                        | $6.16 \times 10^7$      | 4 - 2       | 2                 |
| Na I    | D <sub>1</sub> | 5895.924237                        | $6.14 \times 10^7$      | 2 - 2       | 2                 |

<sup>c</sup> Wavelength references are (1) Morton (2003), (2) Wolf et al. (2008)

Since these two resonance lines are completely dominating the radiation force on Na I, we computed the optical depth  $\tau(v_j)$  for the D<sub>2</sub> line and the effective  $\beta(v_j) = \beta_{\text{NaI}}(\exp[-\tau(v_j)]/3 + \exp[-\tau(v_j)/2]/3)$ , where  $\beta_{\text{NaI}}$  is the radiation force coefficient on Na I without extinction.

### 3. HARPS DATA

To test how well the ion braking scenario compares to observations, we retrieved 489 spectra of  $\beta$  Pic from the ESO archive. The spectra were obtained by HARPS at the ESO 3.6 m telescope at La Silla, Chile, during the period of 2003-10-28 to 2008-03-21. HARPS is a fiber-fed high-resolution ( $R \sim 10^5$ ) echelle spectrograph ( $\lambda = 3800 - 6900 \text{\AA}$ ), dedicated to the search for exoplanets. The long-term radial velocity accuracy of HARPS is estimated to be  $\lesssim 1 \text{ m s}^{-1}$  (Mayor et al. 2003). The HARPS archive at ESO contains data processed by the HARPS science-grade reduction pipeline, producing high-quality extracted wavelength-calibrated spectra. Our main interest are regions around the Ca II H & K doublet at 3934  $\text{\AA}$  and 3968  $\text{\AA}$ , the Fe I 3860  $\text{\AA}$  line, and the region around the Na I D doublet at 5890  $\text{\AA}$  and 5896  $\text{\AA}$  (see Table 1 for line details). Typical signal to noise ratios in single spectra range from 50-100 for the 3900  $\text{\AA}$  region, to 100-250 around 5900  $\text{\AA}$ , depending on exposure time and seeing.

#### 3.1. Cleaning telluric lines

With the high-quality reduced data produced by the HARPS pipeline, not much post processing needs to be done, in general. The exception is the Na I absorption region at 5890  $\text{\AA}$ , where abundant time-varying absorption features from atmospheric H<sub>2</sub>O interfere with the CS absorption lines of interest. Common practice is to remove the telluric features by observing a nearby “telluric standard” right before or after the science observation, and divide out the features (e.g., Vacca et al. 2003). Another is to fit a theoretical atmosphere spectrum (Seifahrt et al. 2010). Since we did not have access to a standard star and it is hard to make a good model fit without leaving systematic residuals, we opted for a third method, making use of the strengths of this particular data set:

1. The supreme stability of HARPS (including the line-spread function).
2. The large number of observations (489).

3. The fact that all telluric absorption lines in the region are optically thin.
4. The variation in position and strength of the telluric features, due to the variable barycentric correction from the orbital and rotation speed of the Earth and the variable airmass and water content of the atmosphere.

By assuming that the stellar spectrum is static and that only the strength and relative shift of the telluric lines are varying, we can use the large number of spectra to constrain the problem. To constrain the telluric absorption lines even further, we downloaded multi-epoch spectra for three additional A0 stars: HD 71155 (40 spectra), HD 177724 (12), and HD 188228 (24). The advantage of A0 stars is that they have very weak Na I features that are rotationally broadened to several 100 km s<sup>-1</sup>, making them suitable as spectrally smooth background lamps to study telluric absorption lines. The problem now becomes to find a (normalized) telluric extinction spectrum  $\kappa(\lambda)$ , a model spectrum  $F_{\text{mod}}^k(\lambda)$  (for each star  $k$ ), and a water column parameter  $\alpha_{k,n}$  (for each observation  $k, n$ ) such that

$$\chi_{\text{mod}}^2 = \sum_k \sum_{n=1}^{N_k} \int_{\lambda} \frac{1}{\sigma_{\text{obs}}^{k,n}(\lambda)} |F_{\text{obs}}^{k,n}(\lambda) - F_{\text{mod}}^k([1 + z_{k,n}]\lambda) \exp(-\alpha_{k,n}\kappa[\lambda])| d\lambda \quad (14)$$

is minimized, where  $N_k$  is the number of observations of star  $k$ ,  $\sigma_{\text{obs}}^{k,n}(\lambda)$  is the error of the measurement of spectrum  $k, n$  at wavelength  $\lambda$ , and  $z_{k,n}$  is the (known) redshift associated with observation  $k, n$ . We implemented a non-linear conjugate gradient minimization method in C++, using the Polak-Ribière method with restart to guarantee convergence (see, e.g., Shewchuk 1994). Since  $\chi^2$  minimization in general is degenerate with respect to a continuous spectrum (i.e. many different spectra can produce the same minimum  $\chi^2$ ), we added a second-order “smoothness” regularization that penalizes rapid changes of the slope:

$$\chi_{\text{reg}}^2(\{f_m\}) = \sum_{m=1}^M \left( \frac{f_{m-1} + f_{m+1}}{2} - f_m \right)^2, \quad (15)$$

where  $f_m$  is the value of pixel  $m$  of the discrete model spectrum (or model extinction) of  $M$  pixels, and  $f_0 = f_{M-1}$  are boundary values (arbitrarily fixed to 1 for stellar spectra and 0 for extinction). In practice we thus minimize

$$\chi^2 = \chi_{\text{mod}}^2 + a\chi_{\text{reg}}^2(\{\kappa_m\}) + b \sum_k \chi_{\text{reg}}^2(\{F_{\text{mod},m}^k\}), \quad (16)$$

where  $a$  and  $b$  are regularization constants that decide the relative importance of the regularization. These constants have to be manually tuned to produce good results; too small and the minimization process will produce numerically noisy spectra, too high and the spectra will be too smooth, devoid of detail. Fortunately, there is a large range between the too small and the too high, that produce good spectra that only weakly depend on the regularization constants. We found that  $a = b = (10 - 1000) \times N_{\text{spec}}$ , where  $N_{\text{spec}}$  is the total

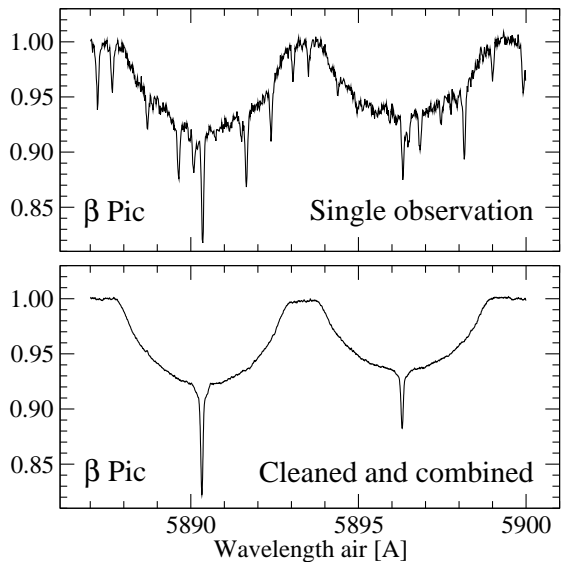


FIG. 1.— The upper panel shows a single spectrum of  $\beta$  Pic as obtained from the HARPS pipeline around the Na I D lines. This region is plagued by numerous telluric absorption lines from H<sub>2</sub>O. The lower panel shows the resulting spectrum from a combination of 92 FEB-free spectra, where the tellurics have been cleaned (as described in §3.1).

number of spectra used, produced good results; in the end, we used  $a = b = 250 \times N_{\text{spec}}$ .

After an optimal fit to the telluric lines were found (simultaneously with the average stellar spectra), we divided (“cleaned”) all individual observations by the fitted telluric extinction. This allows us to inspect individual clean spectra and accommodate potential changes between epochs. The improvement from the cleaning process is illustrated in Fig. 1.

### 3.2. Deriving line profiles

In addition to the stable gas absorption lines seen against  $\beta$  Pic, some lines are known to show strongly velocity-shifted transient absorption features (Lagrange et al. 1987). These absorption features are thought to be originating from “falling evaporating bodies” (FEBs) close to the star (Beust et al. 1989), and are mostly observed in the UV (Deleuil et al. 1993) and in the Ca II H and K lines. Their relevance to the present work is that we want to avoid spectra with strong FEB features, as they may bias the line profiles we are studying. Fortunately, neither Na I nor Fe I are known to show FEB features, but that is likely a sensitivity issue. Since Ca, Na, and Fe around  $\beta$  Pic are strongly ionized (ZBW10), the column density of Ca II is much higher than either Na I or Fe I, making the Ca II H and K lines strongly saturated and FEB features in those lines stronger, despite having oscillator strengths similar to the Na I and Fe I resonant transitions. To reduce the possibility of FEBs affecting the Na I and Fe I line profiles, we inspected all 489 spectra for FEB features in the sensitive Ca II lines, and selected 95 without any sign of FEB activity<sup>1</sup>. With no FEBs visible in the Ca II lines, we

<sup>1</sup> In order to provoke a FEB signal in the Na I lines, we also selected a sample of 262 spectra that show strong red-shifted FEB activity in Ca II. Adding the frames, the resulting Na I indeed shows a red-shifted FEB feature with an equivalent width  $0.8^{+0.8}_{-0.4}$  mÅ, i.e. at the  $\sim 10\%$  level of the main stable line.

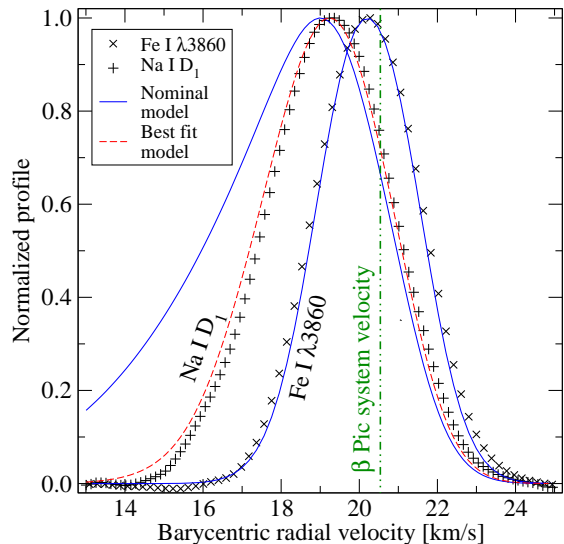


FIG. 2.— The observed normalized line profiles of Na I D<sub>1</sub> and Fe I  $\lambda$ 3860 with over plotted models. The crosses show the observed Fe I line profile, the plus signs the observed Na I line, and the solid lines are from the nominal model (described in §4). As seen, the blue wing of the Na I line is greatly overestimated by the model compared to the observed profile, while the Fe I line looks fine. The dashed line shows the best-fit model for Na I, where the carbon abundance has been increased by a factor of 2 compared to the nominal case (the Fe I profile does not change; see §5). The expected errors on the measured profiles are 1% of the peak for Na I and 3% of the peak for Fe I (see §3.2).

expect their contribution to the Na I and Fe I lines to be negligible. Subregions of the 95 spectra around the Na I 5890 Å, Fe I 3824 Å, and Fe I 3860 Å lines were then extracted and interpolated to a velocity scale of  $0.1 \text{ km s}^{-1}$  resolution (using the HARPS wavelength calibration and line center wavelengths from Table 1), stacked (weighted by their signal to noise), and finally normalized. The resulting profiles for Fe I 3860 Å and Na I 5890 Å are shown in Fig. 2. As seen in the figure, there is a significant offset between the observed radial velocities of Na I and Fe I, as expected from the ion-braking scenario.

Given the large number of high signal-to-noise spectra being combined, errors in the derived profiles are expected to be dominated by systematic errors, such as flat-fielding, flux calibration, and telluric line modeling errors. To check the reliability of the derived profiles, we compared two lines from the same element with each other; many of the expected systematic effects should change with wavelength. One notable exception is contamination in the line profile due to FEB activity; since only spectra without FEBs visible in the Ca II are selected, we estimate the impact on the Fe I/Na I regions to be  $< 1\%$ . By comparing the Fe I 3824 Å with the 3860 Å line, we find them to be consistent to within 3% (1 standard deviation) of the peak. Making the same comparison between the Na I 5890 Å and 5896 Å lines, we find them to be within 1% of each other. The relative radial velocity error is negligible in comparison to the line profile; it is dominated by the  $10 \text{ m s}^{-1}$  accuracy by which the Fe I lines are known (HARPS instrumental errors are  $\lesssim 1 \text{ m s}^{-1}$ ). This means that the velocity difference between the Fe I and Na I lines, which from Fig. 2 is seen to be on the order of  $1 \text{ km s}^{-1}$ , is  $100\times$  larger than the estimated velocity uncertainty, and therefore highly

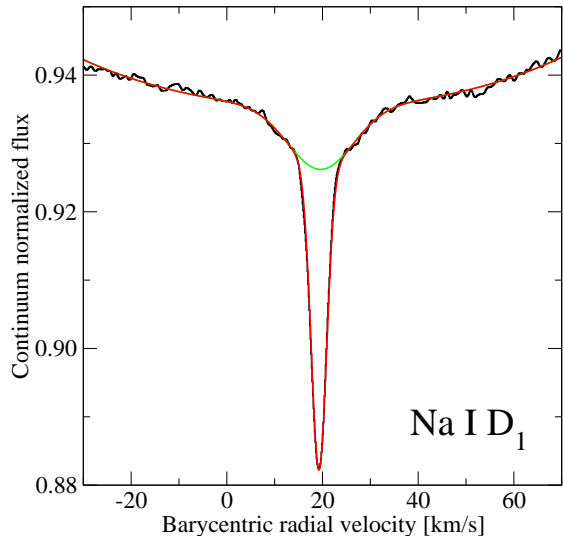


FIG. 3.— The central part of the Na I D<sub>1</sub> line. The curves over plotted the data are the rotational+IS+CS profile, and the rotational+IS profile (used to fit the continuum for the CS line). See § 3.3.

significant.

### 3.3. Removing interstellar absorption

The narrow CS absorption lines in Fig. 1 are seen to have “shoulders”, which are stable in time and due to interstellar (IS) extinction (Vidal-Madjar et al. 1986). To remove them from the profile, we assumed they were Gaussian shaped, and simultaneously fit a rotational profile with two Gaussians per Na line, one for the the CS and IS contribution, respectively (Fig. 3). The rotational profile was best fit by  $v \sin i = 126 \pm 1 \text{ km s}^{-1}$  and a limb-darkening coefficient  $\epsilon = 0.57 \pm 0.06$ . The ratio between the two IS D<sub>2</sub> and D<sub>1</sub> line strengths is 2.0, indicating optically thin absorption. The IS lines are centered at a heliocentric radial velocity of  $19.46 \pm 0.27 \text{ km s}^{-1}$  (i.e. close to the stellar velocity at  $20.5 \text{ km s}^{-1}$ ) and are unusually broad with a broadening parameter  $b = 21.4 \pm 1.7 \text{ km s}^{-1}$ , related to the standard deviation  $\sigma$  of the normal distribution through  $b = 2^{1/2}\sigma$ . Vidal-Madjar et al. (1986) found the IS line to be present also in the nearby star  $\alpha$  Pic and were able to remove it from their  $\beta$  Pic spectrum (along with telluric lines) by dividing the  $\beta$  Pic spectrum with that from  $\alpha$  Pic. Since we do not have access to an  $\alpha$  Pic spectrum of a quality similar to the  $\beta$  Pic spectra, we remove the IS line by division with the fitted Gaussian.

### 3.4. Estimating the line-spread function

To compare the theoretical line profile models with the data, we need to convolve the models with the instrumental profile of the spectrograph, the line-spread function (LSF). One way to estimate the LSF is to measure the shapes of spectral lines from a Th-Ar lamp, since they are expected to be unresolved. Because HARPS records Th-Ar spectra in a parallel fiber with (almost) all science observations, we have a huge data set of spectral lines to choose from. Since we are interested in spectral regions around  $3900 \text{ \AA}$  and  $5900 \text{ \AA}$ , we decided to determine the LSF for those two regions separately by only selecting suitable lines (unblended lines of sufficient flux

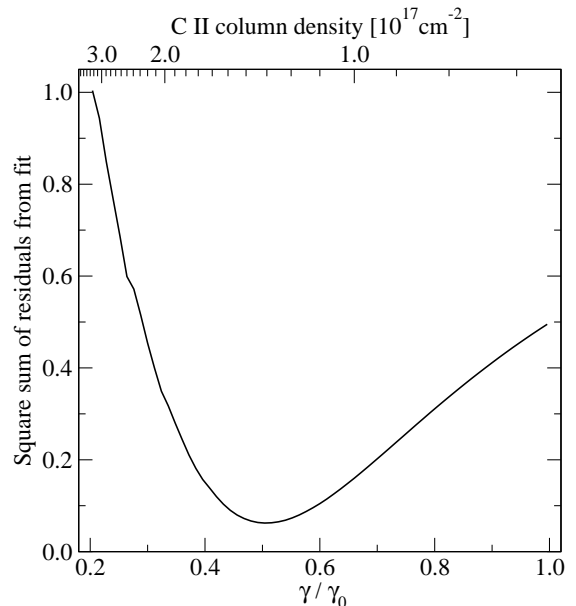


FIG. 4.— Using a model where the ionization velocity  $v_{\text{ion}}$  is reduced as much as possible while still being barely consistent with observations, we here plot the square sum of the residuals between a fit of a particular  $\gamma$  as a function of  $\gamma/\gamma_0$ , with  $\gamma_0$  being the nominal value. The corresponding column densities are given on the upper horizontal axis.

that do not come close to saturate) from the respective orders. With over 500 spectra retrieved from the archive, we ended up with several thousand lines for each region. The lines were then linearly interpolated and shifted to a grid of  $0.1 \text{ km s}^{-1}$  resolution, using the wavelength calibration provided by the HARPS pipeline. Finally, the lines were added, weighted by the signal to noise, fit by a third-degree polynomial (for the background) + a double Gaussian of the functional form

$$\text{LSF}(v) = \sum_{i=1,2} k_i \exp\left(-\frac{[v - m_i]^2}{2\sigma_i^2}\right) \quad (17)$$

where  $v$  is the velocity shift from the center of the line, and the other constants are fitted. Comparing the LSFs determined for the  $3900 \text{ \AA}$  and  $5900 \text{ \AA}$  regions, we found no significant difference ( $<1\%$  of the peak). The fitted parameters  $k_1 = 1.193$ ,  $m_1 = 5.64 \text{ m s}^{-1}$ ,  $\sigma_1 = 1.135 \text{ km s}^{-1}$ ,  $k_2 = -0.194$ ,  $m_2 = -9.01 \text{ m s}^{-1}$ , and  $\sigma_2 = 0.680 \text{ km s}^{-1}$  approximate the LSF very well, with residuals again below  $1\%$  of the peak. The full-width half maximum (FWHM) of the LSF is  $2.67 \text{ km s}^{-1}$ , meaning a spectral resolution of  $R \sim 112\,000$ .

## 4. ANALYTIC METHODS

With a stellar mass of  $M_\star = 1.75 M_\odot$  (Crifo et al. 1997), FBW06 compute  $\beta_{\text{NaI}} = 360 \pm 20$ ,  $\beta_{\text{FeI}} = 27 \pm 2$ ,  $\Gamma_{\text{NaI}}(100 \text{ AU}) = 1.1 \times 10^{-7} \text{ s}^{-1}$  and  $\Gamma_{\text{FeI}}(100 \text{ AU}) = 5.8 \times 10^{-8} \text{ s}^{-1}$ , resulting in  $v_{\text{ion}}^{\text{NaI}} = 3.3 \text{ km s}^{-1}$  and  $v_{\text{ion}}^{\text{FeI}} = 0.5 \text{ km s}^{-1}$ . As our nominal gas disk model, we use the  $\beta$  Pic model with parameters described in ZBW10. Assuming free acceleration, the associated line profiles of Eq. 5 are adjusted for the radial velocity of  $\beta$  Pic by fitting the Fe I profile (as seen in Fig. 2; the fitted radial velocity of the system is  $20.5 \pm 0.2 \text{ km s}^{-1}$ ). The theoretical profile looks fine for Fe I and the red wing of

Na I, but the modeled Na I blue wing is clearly more extended than the observed. Apparently the Na atoms of the  $\beta$  Pic disk do not reach as high speeds as we expect before getting ionized. The discrepancy between model and observations could be due to the following three reasons:

1. Less acceleration, e.g., an overestimated  $\beta$  value for Na I. Since the  $\beta$  Pic spectrum is very well constrained around the Na I D lines, however, and the corresponding radiative transition coefficients are known to very high accuracy for these resonance lines, it is unlikely that the  $\beta$  value is more off than the estimated 8%.
2. Higher ionization rate of Na I. This will give less time for the atom to accelerate before getting ionized. The ionization rate is directly proportional to the ionizing UV radiation from the star. The UV part of the  $\beta$  Pic spectrum is not well constrained outside the spectral windows observed by FUSE (905–1187 Å) and HST/STIS (1459–2888 Å), but most of the ionizing photons are expected to arise from close to the ionization threshold at 2413 Å, where the spectrum is known to within 10% from STIS (Aki Roberge, priv. comm. 2010). The ionization model of ZBW10 reproduce observed ionization ratios in the  $\beta$  Pic gas disk reasonably well, so a much different ionization rate than the assumed would be surprising.
3. More efficient braking. With stronger braking, the resulting drag velocity is smaller. The braking is the strongest for the higher speed particles, possibly explaining the observed absence of a strong blue wing. Since the braking is dominated by, and directly proportional to, the number density of C II, an underestimate of C II would result in a proportional underestimate of the braking force. Strongly saturated absorption lines of C II observed by FUSE (ROB06) have determined the C abundance in the  $\beta$  Pic disk to be at least 20 $\times$  overabundant with respect to other elements in the disk at cosmic abundance. Since the stable CS lines are saturated and blended with a time-variable broad component due to FEBs, small variations in the intrinsic line shape can mimic large abundance changes. It thus seems motivated to explore the possibility that the carbon is even more overabundant than previously thought, and what consequences that has for the braking and the line profile of Na I.

A combination of the above is also possible. In particular, should braking be more efficient than anticipated, the lower radial velocities will contribute to stronger self-shielding and a decrease in the  $\beta$ -value, resulting in less acceleration.

To investigate the possible scenarios producing the observed line profiles, we made an extensive parameter search for  $v_{\text{ion}}$  and  $\gamma$ , trying to fit the profile from Eq. 10 to the observations (leaving the system radial velocity as a free parameter). Because self-shielding, as explored in the numerical model, in most of the parameter space is very small (with an optical depth less than 0.1 resulting in only a minor correction to the analytical profile), we

only used the numerical model to investigate a subset of models where self-shielding was expected to be most important.

## 5. RESULTS AND DISCUSSION

Since the expected radial velocity increases with both  $v_{\text{ion}}$  and  $\gamma$ , and since the observed line profiles are not well resolved, the problem of finding the optimal  $v_{\text{ion}}$  and  $\gamma$  becomes ill-conditioned. Even so, we can constrain the parameter space by finding what combinations of parameters are consistent with the line profiles. One question is if additional braking is necessary, or if a moderation of  $v_{\text{ion}}$  by stretching known quantities within their estimated uncertainties is sufficient to explain the profile. This should put a lower limit on the extra braking needed, and by extension put an independent lower limit on the C II content in the disk. We get a lower reasonable limit for the  $v_{\text{ion}}$  of Na I by assuming  $\beta = 330$  (which is  $1.5\sigma$  below its estimated value) and an ionization rate that is 20% higher than the nominal, resulting in  $v_{\text{ion}} = 2.5 \text{ km s}^{-1}$ . In Fig. 4 the least square-sum of the residuals between the observed line profiles for Na I and Fe I, and their models (where the system radial velocity again was a free parameter) are plotted as a function of  $\gamma/\gamma_0$ , where  $\gamma_0$  corresponds to the  $\beta$  and  $\Gamma$  assumed above, and a braking ion gas density according to the model by ZBW10. The corresponding column density of C II is given on the upper horizontal axis of the figure. The smallest residuals are found for  $\gamma/\gamma_0 = 0.5$ , corresponding to the C II column density  $N_{\text{C II}} = 1.3 \times 10^{17} \text{ cm}^{-2}$ , which is  $2\times$  the model column density of ZBW10, and  $6\times$  the  $N_{\text{C II}} = 2.0_{-0.4}^{+2.1} \times 10^{16} \text{ cm}^{-2}$  reported by ROB06. The best-fit Na I velocity profile resulting from increased braking is shown in Fig. 2. Because the braking is proportional to the velocity, only the high-velocity tail of the profile is significantly affected by the C II density increase. Similarly, Fe I never gets accelerated to high enough velocities for braking to be important, so the Fe I velocity profile does not change with the increased C II density.

The implicated overabundance of C is on the order of 100 $\times$  compared to cosmic abundances of other detected elements. Perhaps this reflects the intrinsic abundance of the gas production mechanism; e.g., Karmann et al. (2003) find carbon rich FEBs essential to explain the high-velocity FEB spectral features. Another possibility is that the current abundances are more strongly dependent on the gas *removal* mechanism. Even with an efficient ion braking mechanism, any specific particle is neutral some fraction of the time. If the radiation pressure on the particles in their neutral state overcomes gravity, they will be accelerated outwards until they get ionized (and braked again). This will effectively remove elements at a rate proportional to their ionization speed  $v_{\text{ion}}$  and neutral fraction. On the other hand, elements that do not experience sufficient radiation pressure in their neutral phase (i.e., H, He, C, N, O, F, Ne, and Ar, see Table 1 of FBW06) are thus expected to pile up, thereby increasing their relative abundance compared to their production abundance. Unfortunately, the elements that experience little radiation pressure are also the elements that are difficult to observe, so only C and O of that group have so far been detected (ROB06),

although H has observed upper limits (Freudling et al. 1995; Lecavelier des Etangs et al. 2001). Surprisingly, absorption line observations by FUSE favor a cosmic abundance of disk O I gas (ROB06). Again, this conclusion is sensitively dependent on the assumed (unresolved) line profile, as can be seen in Fig. 1 of the ROB06 online supplementary material: reducing the broadening parameter from the best-fit value of  $\sim 14 \text{ km s}^{-1}$  to a few  $\text{km s}^{-1}$  results in a much higher, but less constrained, column density. A broadening parameter as large as  $14 \text{ km s}^{-1}$  for the stable disk gas is unexpected in itself considering other observed absorption lines, and is likely caused by multiple unresolved velocity components from FEBs (as seen for other elements).

One way to confirm the overabundance of C II around  $\beta$  Pic is to observe its thermal  $157.7 \mu\text{m}$  emission, as the emission is predicted to be roughly proportional to the C gas mass (ZBW10). The *Infrared Space Observatory* (ISO) observed  $\beta$  Pic with the LWS instrument and found a  $4\sigma$  emission feature with an integrated flux of  $10^{-13} \text{ erg s}^{-1} \text{ cm}^{-2}$  (Kamp et al. 2003). This is  $15\times$  more emission than predicted from a gas disk with  $20\times$  overabundant C (ZBW10), and would imply a C abundance of  $>100\times$  over cosmic values (compared to other observed elements in the disk). Recently, the infrared space telescope *Herschel* with the PACS instrument observed both C II  $157.7 \mu\text{m}$  and O I  $63.2 \mu\text{m}$  emission, confirming the ISO detection and finding that O I probably also is overabundant. The data are still being analyzed, however, as e.g. the spectrophotometric calibration is not settled yet. A publication presenting the *Herschel* observations is in preparation by the key project *Stellar Disk Evolution* team lead by G. Olofsson.

The processes that produce the C-rich gas disk around  $\beta$  Pic must reasonably be present also in other debris disk systems. The frequency and efficiency of the process is not known, but the absence of detectable amounts of gas around AU Mic (Roberge et al. 2005), another edge-on debris disk system in the  $\beta$  Pic moving group, shows that the process is not ubiquitous. A model to quantitatively investigate the balance of gas production and removal mechanisms in debris disks will be the subject for future studies.

## 6. CONCLUDING SUMMARY

The prediction made by the braking model of FBW06, that Fe I and Na I should show different radial velocities, is confirmed. This shows that, to a first order approximation, neutral elements are not braked by the gas, while the ions must be. Looking more closely at the line profiles, we see an absence of a Na I high-velocity population, expected from free acceleration. Our interpretation is that the high-velocity Na atoms must be braked. A factor of  $2\text{--}5\times$  more C II gas than previously estimated is required for C II to be the braking agent; the implication is that the gas disk around  $\beta$  Pic is even more C rich than previously thought, up to  $100\times$  cosmic abundance relative to other detected elements.

The author acknowledges the useful discussions with Jean-Michel Désert, Ricky Nilsson, Göran Olofsson, Seth Redfield, Aki Roberge, Philippe Thébault, and Yanqin Wu. This work was supported by the *Swedish National Space Board* (contract 84/08:1).

## REFERENCES

- Aumann, H. H. 1985, *PASP*, 97, 885  
 Backman, D. E., & Paresce, F. 1993, in *Protostars and Planets III*, ed. E. H. Levy & J. I. Lunine, 1253–1304  
 Beust, H., Lagrange-Henri, A. M., Vidal-Madjar, A., & Ferlet, R. 1989, *A&A*, 223, 304  
 Brandeker, A., Liseau, R., Olofsson, G., & Fridlund, M. 2004, *A&A*, 413, 681  
 Chen, C. H., Li, A., Bohac, C., et al. 2007, *ApJ*, 666, 466  
 Crifo, F., Vidal-Madjar, A., Lallement, R., Ferlet, R., & Gerbaldi, M. 1997, *A&A*, 320, L29  
 Czechowski, A., & Mann, I. 2007, *ApJ*, 660, 1541  
 Deleuil, M., Gry, C., Lagrange-Henri, A., Vidal-Madjar, A., Beust, H., Ferlet, R., Moos, H. W., Livengood, T. A., Ziskin, D., & Feldman, P. D. 1993, *A&A*, 267, 187  
 Fernández, R., Brandeker, A., & Wu, Y. 2006, *ApJ*, 643, 509  
 Freudling, W., Lagrange, A., Vidal-Madjar, A., Ferlet, R., & Forveille, T. 1995, *A&A*, 301, 231  
 Hobbs, L. M., Vidal-Madjar, A., Ferlet, R., Albert, C. E., & Gry, C. 1985, *ApJ*, 293, L29  
 Kamp, I., van Zadelhoff, G.-J., van Dishoeck, E. F., & Stark, R. 2003, *A&A*, 397, 1129  
 Karmann, C., Beust, H., & Klinger, J. 2003, *A&A*, 409, 347  
 Lagrange, A.-M., Beust, H., Mouillet, D., et al. 1998, *A&A*, 330, 1091  
 Lagrange, A. M., Ferlet, R., & Vidal-Madjar, A. 1987, *A&A*, 173, 289  
 Lecavelier des Etangs, A., Vidal-Madjar, A., Roberge, A., et al. 2001, *Nature*, 412, 706  
 Mayor, M., Pepe, F., Queloz, D., Bouchy, F., Rupprecht, G., et al. 2003, *The Messenger*, 114, 20  
 Mentuch, E., Brandeker, A., van Kerkwijk, M. H., Jayawardhana, R., & Hauschildt, P. H. 2008, *ApJ*, 689, 1127  
 Morton, D. C. 2003, *ApJS*, 149, 205  
 Olofsson, G., Liseau, R., & Brandeker, A. 2001, *ApJ*, 563, L77  
 Roberge, A., Feldman, P. D., Weinberger, A. J., Deleuil, M., & Bouret, J.-C. 2006, *Nature*, 441, 724  
 Roberge, A., Weinberger, A. J., Redfield, S., & Feldman, P. D. 2005, *ApJ*, 626, L105  
 Seifahrt, A., Käufel, H. U., Zängl, G., Bean, J. L., Richter, M. J., & Siebenmorgen, R. 2010, *ArXiv e-prints*  
 Shewchuk, J. R. 1994, *An Introduction to the Conjugate Gradient Method Without the Agonizing Pain*, Tech. rep., Pittsburgh, PA, USA  
 Slettebak, A. 1975, *ApJ*, 197, 137  
 Smith, B. A., & Terrile, R. J. 1984, *Science*, 226, 1421  
 Vacca, W. D., Cushing, M. C., & Rayner, J. T. 2003, *PASP*, 115, 389  
 van Dishoeck, E. F., & Black, J. H. 1988, *ApJ*, 334, 771  
 van Leeuwen, F. 2007, *A&A*, 474, 653  
 Vidal-Madjar, A., Ferlet, R., Hobbs, L. M., Gry, C., & Albert, C. E. 1986, *A&A*, 167, 325  
 Vidal-Madjar, A., Lagrange-Henri, A., Feldman, P. D., et al. 1994, *A&A*, 290, 245  
 Wolf, A. L., van den Berg, S. A., Gohle, C., Salumbides, E. J., Ubachs, W., & Eikema, K. S. E. 2008, *Phys. Rev. A*, 78, 032511  
 Zagorovsky, K., Brandeker, A., & Wu, Y. 2010, *ApJ*, 720, 923  
 Zuckerman, B., Song, I., Bessell, M. S., & Webb, R. A. 2001, *ApJ*, 562, L87